

SUPPLEMENTAL MATERIALS

Title

Novel Mouse Model of Myocardial Infarction, Plaque Rupture and Stroke Shows Improved Survival with Myeloperoxidase Inhibition

Authors

*Sohel Shamsuzzaman, PhD¹; *Rebecca A. Deaton, PhD¹; Anita Salamon, MSc^{1,2}; Heather Doviak, BS, MPS³; Vlad Serbulea, PhD^{1,4}; Victoria M. Milosek, MSc^{1,5}; Megan A. Evans, PhD³; Santosh Karnewar, PhD¹; Subhi Saibaba^{1,6}; Gabriel F. Alencar, PhD⁷; Laura S. Shankman, PhD¹; Kenneth Walsh, PhD^{2,3}; Stefan Bekiranov, PhD³; Olivier Kocher, MD, PhD⁸; Monty Krieger, PhD⁹; Bengt Kull, BSc¹⁰; Marie Persson, BSc¹¹; Erik Michaëlsson, PhD¹²; Nils Bergenhem, PhD¹³; Sepideh Heydarkhan-Hagvall, PhD¹⁴; #Gary K. Owens, PhD^{1,5}

Affiliations

- ¹ Robert M. Berne Cardiovascular Research Center, University of Virginia School of Medicine, Charlottesville, VA, USA.
- ² Department of Biochemistry and Molecular Genetics, University of Virginia School of Medicine, Charlottesville, VA, USA.
- ³ Hematovascular Biology Center, Robert M. Berne Cardiovascular Research Center, University of Virginia School of Medicine, Charlottesville, VA, USA.
- ⁴ Department of Pharmacology, University of Virginia School of Medicine, Charlottesville, VA, USA.
- ⁵ Department of Molecular Physiology and Biophysics, University of Virginia, Charlottesville, VA, USA.

- ⁶ Program in Fundamental Neuroscience, University of Virginia, Charlottesville, VA, USA.
- ⁷ Beirne B Carter Center for Immunology Research, University of Virginia School of Medicine, Charlottesville, VA, USA.
- ⁸ Department of Pathology and Center for Vascular Biology Research, Beth Israel Medical Deaconess Medical Center Harvard Medical School, Boston, MA, USA.
- ⁹ Department of Biology, Massachusetts Institute of Technology, Cambridge, MA, USA.
- ¹⁰ BioPharmaceuticals R&D Early Cardiovascular Renal and Metabolism (CVRM) Bioscience Cardiovascular, AstraZeneca, Mölndal 43183, Sweden.
- ¹¹ BioPharmaceuticals R&D Early Cardiovascular Renal and Metabolism (CVRM) DMPK, AstraZeneca, Mölndal 43183, Sweden.
- ¹² Early Clinical Development, Research and Early Development, Cardiovascular, Renal, and Metabolism, Biopharmaceuticals R&D, AstraZeneca, Gothenburg, Sweden.
- ¹³ Alliance Management, Business Development & Licensing, BioPharmaceuticals R&D, AstraZeneca, Waltham, MA, USA.
- ¹⁴ AstraZeneca R&D, Chief Medical Office, Global Patient Safety, Pepparedsleden 1, Mölndal, SE43183, Sweden.

***S. Shamsuzzaman and R.A. Deaton contributed equally.**

Short Title: Mouse Model of Spontaneous Heart Attack and Stroke

Corresponding author:

Dr. Gary K. Owens

Email: gko@virginia.edu

University of Virginia School of Medicine

Robert M. Berne Cardiovascular Research Center

PO Box 801394

Charlottesville, Virginia 22908-1394

Phone: 434-924-5993

Contents:

Supplemental Methods

Figures S1-S12

Major Resources Table

References 23-24,29,44,57,77-81

Supplemental Methods

Rodent Diet and Animal Monitoring

To induce SMC-specific lineage tracing, *Myh11-CreER^{T2}-eYFP* SR-BI^{ΔCT/ΔCT}/*Ldlr*^{-/-} (henceforth abbreviated as “SR-BI^{ΔCT/ΔCT}/*Ldlr*^{-/-}”) mice were fed a tamoxifen diet (250 mg of tamoxifen/kg diet) (Envigo; Catalog# TD.130856) *ad libitum* starting at 6-8 weeks of age to activate *Myh11*-driven Cre recombinase (**Figure 1A**). Following tamoxifen feeding and one week of rest (to ensure tamoxifen clearance), mice were fed standard rodent chow diet (Teklad; Catalog# 7912), an atherogenic Western diet (WD) (containing 21% fat, 0.2% cholesterol) (Envigo; Catalog# TD.88137) or WD formulated with AZM198 to achieve a daily dose of 500 μmol/kg based on daily food consumption of 10% of body weight as described in previous murine studies.⁵⁷

SR-BI^{ΔCT/ΔCT}/*Ldlr*^{-/-} mice (or their wild-type or heterozygous littermates) were fed *ad libitum* starting at 9 weeks of age until they reached a humane terminal endpoint or a maximum of 26 weeks of diet feeding (35 weeks of age). Mice were carefully monitored by trained vivarium caretakers and researchers to recognize signs of MI and stroke including decreased activity, ruffled coat, hunched posture, labored breathing, unsteady gait, hind limb paralysis and head tilt/spinning. If any of the above signs were noticed during monitoring, mice were further examined by trained veterinary technicians. If signs of MI/stroke or pain/distress were not able to be alleviated by a

veterinary technician, euthanasia was recommended, and this was considered the humane terminal endpoint. The animal was immediately euthanized by CO₂ asphyxiation.

All sections of this report adhere to the ARRIVE guidelines for reporting animal research.⁷⁷

Tissue and Plasma Collection and Processing

After euthanasia by CO₂ asphyxiation, blood was collected in K₂ EDTA blood collection tubes for complete blood count (CBC) and plasma isolation (described below). Mice were then gravity-perfused via the left ventricle of the heart with 5 mL of PBS, 10 mL of 4% paraformaldehyde (PFA) (EMS; Catalog# 15710) in PBS, and an additional 5 mL of PBS. Organs were collected, weighed, and digitally photographed. Tissues were fixed for 24 hours in 4% PFA in PBS with gentle shaking followed by processing and paraffin embedding.

Blood Analysis

For complete blood count (CBC), blood was collected in K₂EDTA microtainer blood collection tubes (BD; Catalog# 363706) and analyzed by the University of Virginia (UVA) Clinical Pathology Laboratory using an automated hematology analyzer (Sysmex; Catalog# XN-9000). For plasma preparation, blood was collected in K₂EDTA vacutainer tube (BD; Catalog# 367856) and mixed on a tube roller for at least for 30 minutes at room temperature (RT). Plasma was prepared by centrifugation at 300xg for 10 minutes at RT and stored at -80°C until analyzed. Lipid panel (total cholesterol, triglycerides, low-density lipoprotein cholesterol [LDL-C], high-density lipoprotein cholesterol [HDL-C]), high sensitivity cardiac troponin I (hs-cTroponin I), alanine transaminase (ALT) and aspartate transaminase (AST) in plasma were analyzed by the UVA Clinical Pathology Laboratory by using automated analyzers (Abbott Alinity c or Alinity i series).

MPO activity, multiplex cytokine analysis and AZM198 concentration in plasma were analyzed by AstraZeneca (Sweden) (described below).

Histology

PFA-fixed paraffin-embedded tissues were sectioned to a thickness of 10 μm . For assessments of MI, the whole heart was sectioned from the apex to the aortic sinus. Following de-paraffinization and rehydration, every 5th section (200 μm apart) was stained with Masson's trichrome (Polysciences; Catalog# 25088-1) to identify myocardial fibrosis (indicative of MI), which stains fibrotic tissue blue and healthy myocardium red. Locations of the myocardial fibrosis were recorded. Fibrosis was quantified by Fiji (ImageJ) software (USA National Institute of Health) as number of blue pixels/sum of blue and red pixels. Myocardial fibrosis was expressed as a percentage of total left ventricle (LV) and right ventricle (RV) area.

Coronary artery atherosclerosis was analyzed in Masson's trichrome stained sections of the heart at the aortic sinus. Coronary artery lesion morphometry and percent occlusion were quantified by Fiji (ImageJ) software as was done previously for BCA lesions.^{24,78} To assess carotid artery and BCA morphometry, Modified Russell-Movat pentachrome staining was performed as previously described.^{24,78} Plaque rupture in coronary artery, carotid artery and BCA was assessed both gross morphologically and histologically by Ter-119 staining of PFA-fixed paraffin embedded sections as previously described.^{24,44} Coronary artery lesions were further assessed by immunofluorescence staining as described below in Immunofluorescence Staining section.

For assessments of ischemic stroke, the fixed paraffin-embedded brains were sectioned (10 μm) from olfactory bulb to cerebellum. Following de-paraffinization and rehydration, standard

hematoxylin and eosin (H&E) staining was carried out to determine the damaged area of the brain. The locations of the ischemic stroke in the brains were recorded. The brain damage due to ischemic stroke was further assessed by immunofluorescence staining using NeuN, Iba1 and GFAP antibodies (described below). In addition, cerebral vessels were assessed by immunofluorescence staining using antibodies to ACTA2 and eYFP (smooth muscle lineage tracing marker) (described below).

For liver histology, PFA-fixed paraffin-embedded tissues were deparaffinized and rehydrated. Liver morphology was assessed by H&E staining. Liver fibrosis was assessed by Picro Sirius Red/Fast green (PSR) staining. To assess lipid deposition, PFA-fixed liver tissues were placed in 30% sucrose for 24 hours followed by embedding in optimal cutting temperature (OCT) compound (Tissue-Tek; Catalog# 4583). OCT-embedded tissues were sectioned to a thickness of 10 μ m. Frozen liver sections were assessed for lipid deposition by Oil Red O staining. Liver fibrosis (PSR⁺ area) and lipid deposition (ORO⁺ area) were expressed as percentage of total liver section area by using Fiji (ImageJ) software.

Immunofluorescence Staining

For Immunofluorescence staining, sections were first deparaffinized in xylene and rehydrated in ethanol. Antigen retrieval was performed as per manufacturer's instructions (Vector Lab; Catalog# H-3300). Sections were blocked in PBS containing fish skin gelatin (6 g/L) and 10% horse serum for 1 hour at room temperature. Tissues were then incubated with the following primary antibodies either overnight at 4°C or 1 hour at room temperature: GFP (Abcam; Catalog# ab6673; 1:100 dilution and Catalog# ab252881; 1:200 dilution), MPO (Abcam; Catalog# ab208670; 1:200 dilution, and R&D; Catalog# AF3667; 1:200 dilution), Cit-H3 (Abcam; Catalog#

ab281584; 1:200 dilution), FITC-conjugated ACTA2 (Sigma; Catalog# F3777 clone 1A4; 1:500 dilution), NeuN (Abcam; Catalog# ab177487; 1:500 dilution), Iba1 (Fujifilm Wako; Catalog# 013-27691; 1:500 dilution), GFAP (Abcam; Catalog# ab7260 and Catalog# ab4674; 1:500 dilution) or their isotype IgG as control. Slides were incubated with DAPI (Invitrogen; Catalog# D21490, 5mg/mL; 1:100 dilution) and one of the following secondary antibodies: Donkey anti-rabbit Alexa Fluor 488 (Invitrogen; Catalog# A21206; 1:250 dilution), Donkey anti-goat Alexa Fluor 647 (Invitrogen; Catalog# A21447; 1:250 dilution), Donkey anti-rabbit Alexa Fluor 546 (Invitrogen; Catalog# A10040; 1:250 dilution), Donkey anti-chicken Alexa Fluor 647 (Jackson ImmunoResearch; Catalog# 703-605-155; 1:250 dilution) for 1 hour at room temperature. Following washing, slides were mounted with coverslips and Prolong Gold Antifade Mountant (Invitrogen; Catalog# P36930). Sections were imaged using a Zeiss LSM880 confocal microscope at either 20x or 40x magnification and 0.6x zoom to acquire a series of z-stack images at 1 μ m intervals. Acquisition settings were determined using the IgG isotype control and were kept constant across images acquired. Maximum intensity projection was used to generate the representative images. Analysis of cellular compositions (*Myh11*-eYFP⁺, ACTA2⁺, *Myh11*-eYFP⁺ACTA2⁺, *Myh11*-eYFP⁺ACTA2⁻) of coronary artery atherosclerosis in whole coronary lesions was performed using Fiji (ImageJ) software and quantified as percent population of either DAPI or *Myh11*-eYFP⁺) as previously analyzed in BCA lesions²⁹. Neutrophil extracellular traps (NETs) were defined by the co-localization of MPO, citrullinated histone 3 (Cit-H3) and DAPI in and were quantified in right carotid artery lesions using Fiji (ImageJ) software.

Echocardiographic Measurements

Serial transthoracic echocardiography was performed at indicated time points using a Vevo 2100 ultrasound system equipped with an MS400 probe (VisualSonics, Fujifilm). Mice were anesthetized with isoflurane in medical air throughout the duration of the procedure: 3-5% for induction and 1-2% for maintenance. At this dose of isoflurane, the heart rates were maintained at approximately 450-550 bpm. Once anesthetized, mice were placed on a heated platform that contained electrocardiogram (ECG) electrode pads. Chest fur was removed with a chemical hair remover, and ultrasound gel was applied. Both parasternal long axis and short axis images were acquired. Fractional shortening (FS) was measured from M-mode images of the short axis view. Analysis was performed using Vevo LAB software (VisualSonics, Fujifilm).

Multiplex Cytokine Analysis

The multiwell assay plate, reagents, diluents, samples, and controls were prepared and used to detect the cytokine expression according to the manufacturer's protocol (V-PLEX Plus Mouse Cytokine 19-Plex; Meso Scale Discovery, Rockville, MD, USA, Catalog# K15048G and K15245G). Briefly, the samples were prediluted 2.5x in kit sample diluent 41, and the standards were serially diluted to generate the standard curve. The Meso Scale Discovery (MSD) plate was washed three times with 200 μ L wash buffer. The samples, standards, and quality controls (50 μ L each) were transferred to the MSD plate and incubated for 2 hours at room temperature with gentle shaking. Afterward, the washing step was repeated. The detection antibody (25 μ L) was added to plate and incubated for 2 hours at room temperature with gentle shaking. The washing step was repeated. 150 μ L reading buffer were added and the values were recorded using MSD Sector Imager S600. Assays were performed using the Beckman Coulter robotic assay system (SCARA

System) that incorporated a Biomek NX Span-8 and Biomek FX double 96-head pipetting robots, Cytomat2 shake incubator, Biotek EL405 washer, and MSD S600 reader.

Plasma AZM198 Analysis

Plasma samples (20 μ l each) were precipitated with 150 μ l acetonitrile and vortexed, followed by a 20 minute centrifugation at 3220xg at 4°C. Supernatants were transferred to a fresh 96 deep-well plate (Nunc 1mL; ThermoFisher Scientific; Catalog# 260252) and diluted 1:1 with water prior to LC-MS analysis. Matrix-matched calibration samples and blanks were prepared as were the study samples. Samples were analyzed using reversed-phase high-pressure liquid chromatography with rapid gradient elution. Compounds were detected using a Waters Xevo TQ-S triple quadrupole mass spectrometer (Waters Corporation, Milford, MA, USA). Chromatographic separation was performed using an ACQUITY BEH C18 1.7 μ M, 2.1x50 mm column with the column temperature set to 40°C. The flow rate was maintained at 0.7 ml/min using a mobile phase of 2% acetonitrile and 0.2% formic acid in water (A) and 0.2% formic acid in acetonitrile (B). The elution gradient was ramped from 4% B to 95% B from 0 to 1.5 min, maintained at 95% B until 2.3 min and finally conditioned from 2.4 to 2.7 min. Mass spectrometry was performed using positive electrospray ionization and multiple reaction monitoring of transition 321.07>136.13 m/z.

MPO Activity Assay

A high-binding, 96-well white plate (Lumitrac, PS flat-bottom; Greiner Bio-One; Catalog# 655074) was coated with 50 μ L mouse anti-MPO capture antibodies (Abcam; Catalog# 16886; 1:200 dilution) and incubated overnight at 4°C. The plate was then washed three times with 350

μ l PBS-Tween (PBS-T) and blocked with 1% BSA in PBS for 1 hour at 4°C. 50 μ L plasma (diluted 1:3 in PBS) were added to each well followed by incubation for 2 hours at 4°C, at which time the plate was washed three times with 350 μ l PBS-T. 50 μ L Amplex Red Assay Buffer [50 mM NaPO₄ pH 7.4, 140 mM NaCl, 10 mM Na₂NO₂, 40 μ M Amplex Red (Invitrogen; Catalog# A12222), 10 μ M H₂O₂] was added, and the plate was incubated in the dark for 25 minutes at room temperature with shaking and then fluorescence was measured using a SpectraMax Paradigm plate reader at excitation and emission wavelengths of 535 nm and 595 nm, respectively. Activity was calculated based on a standard curve determined using purified recombinant mouse MPO protein (R&D Systems; Catalog# 3667-MP). The MPO activity was adjusted for the concentration of MPO by dividing the detected MPO activity with MPO concentration determined separately by ELISA (HyCult Biotech; Catalog# HK210).

Sample Processing, Sequencing and Data Analysis for Bulk RNAseq

Liver tissues from SR-BI ^{Δ CT/ Δ CT}/*Ldlr*^{-/-} mice fed either WD (n = 5) or WD+AZM198 (n = 6) for 8 weeks were flash frozen in liquid nitrogen for RNA-seq analysis. Tissue (~30 mg in 600 μ l of RLT lysis buffer with β -ME) was homogenized using TissueLyser II (Qiagen) at 30 Hz for 6 minutes. RNA was extracted from homogenate using RNeasy Plus Mini Kit (Qiagen; Catalog#74136), including the gDNA eliminator column. Sequencing was performed on the NovaSeq X Plus sequencing system at Novogene (Sacramento, California) with specifications of a total data output of 9Gb. FASTQ files were aligned to a custom mouse reference genome, mm39 (Genome assembly GRCm39). Data analysis was conducted in R (version 4.2.1) as previously described.^{24,78} Briefly, 150nt paired-end reads were mapped to the mm39 reference genome (Genome assembly GRC m39) using STAR v2.7. The Subread package, FeatureCounts, was used

to generate a table of gene counts/quantification. Differentially expressed genes were identified using DESeq2 Bioconductor R package (version 1.38.3) using a 5% ($P_{adj} < 0.05$) false discovery rate. Benjamini-Hochberg was used to adjust P values to less than or equal to the 5% false discovery rate. Reactome pathways analysis was performed on all significantly up- or downregulated genes based on P_{adj} value (\log_2 fold change > 1 ; $P_{adj} \leq 0.05$). Enrichment significance was quantified using $-\log_{10}$ of P_{adj} .

Lipidomic Analysis of Livers

SR-BI $^{\Delta CT/\Delta CT}/Ldlr^{-/-}$ mice were fed either WD or WD+AZM198 for 8 weeks and liver lobes were collected, snap-frozen in liquid nitrogen and submitted to Novogene (Sacramento, California) for lipidomic analysis. Briefly, 10 mg of tissue was homogenized in 1 mL of methyl-tert-butyl ether (MTBE): methanol (3:1), premixed with internal standards. After mixing and centrifugation, the upper layer was removed and dried down under nitrogen. The sample was reconstituted with 200 μ L of acetonitrile:isopropyl alcohol (1:1), mixed, and centrifuged. 120 μ L of supernatant was used for ultra-performance liquid chromatography-tandem mass spectrometry (UPLC-MS/MS) (QTRAP 6500+; SCIEX) analysis.

Cell Processing and Data Analysis for scRNAseq

Cell processing: Four samples (unsorted and eYFP $^{+}$ sorted cells from pooled BCA lesion area) from three WD-fed or three WD+AZM198-fed SR-BI $^{\Delta CT/\Delta CT}/Ldlr^{-/-}$ mice were prepared as previously described and briefly summarized below.^{23,24} Mice were euthanized by CO $_2$ asphyxiation and perfused with 20 mL of PBS + 1 μ g/mL Actinomycin-D. BCA lesion regions (as shown in **Figure 7A**) were excised and placed into FACS buffer (1% BSA in PBS) on ice until all

samples were collected. Tissues were chopped with scissors and digested in a cocktail containing 4 units/mL LiberaseTM (Roche; Catalog# 355374) and 0.744 units/mL Elastase (Worthington Bio. Corp: Catalog# LS002279) in RPMI + 1 µg/mL Actinomycin-D for 60 min at 37°C. Individual samples were pooled (3 WD-fed mice pooled and 3 WD+AZM198-fed mice pooled). A subset of pooled cells was taken for the “unsorted” sample and the remaining pooled cells were used for the “eYFP⁺” sample which were sorted using a BD InfluxTM Cell Sorter. Live cells from “unsorted” and “eYFP⁺ sorted” samples were counted and submitted directly for scRNAseq library preparation.

Sequencing, read alignments, and quality control: All Libraries were prepared using the Chromium Next GEM Single Cell 3' Kit v3.1 (v3 Chemistry) at the Genome Analysis and Technology Core at the University of Virginia, in accordance with the manufacturer's instructions. 400M reads/cell and ~2000 cells per sample were targeted. Sequencing was performed on the NovaSeq 6000 sequencing system (Illumina) at Novogene (Sacramento, California) with system specifications of paired-end reads at 150bp length (PE150) and a total data output of 468 Gb.

FASTQ files were aligned using the cellranger count pipeline (version 6.0.1) to a custom mouse reference genome, mm10 (GENCODE vM23/Ensembl 98). This custom reference was established with cellranger mkref (version 6.0.1) by incorporating the FASTA and GTF files of the reporter gene (eYFP) into the mouse genome.

Data analysis was conducted in R (version 4.1.1) utilizing Seurat 4.3.01. WD groups (unsorted and sorted samples) exhibited a median of 11,949 and 15,300 UMIs per cell and 2,877 and 3,620 genes per cell, respectively. In contrast, the WD+AZM198 groups displayed medians of 6,922 and 18,919 UMIs per cell and 1,967 and 3,838 genes per cell, respectively. Uniform filtering parameters were applied to all samples. Cells expressing genes within the range of 420–

5800, denoting the 5th to 95th percentile, were considered. Cells with over 15% of reads originating from mitochondrial genes and over 5% from hemoglobin genes were categorized as poor quality and excluded.

Clustering, annotation, and pathway analysis: The gene counts were normalized using SCTransform.⁷⁹ To compromise between accuracy and computational needs of the dataset, two metrics were applied to select number of principal components (PCs), which were: 1) PCs that cumulatively contribute 90% of the standard deviation, and 2) the point where the percent change in variation between the consecutive PCs is more than 0.05%. Based on analysis, the PC range spanned from 26 to 41, with 28 being chosen for clustering. To cluster and visualize all cells, a Louvain algorithm was used. ChooseR⁸⁰ tool was used to determine the silhouette scores and identified range of resolutions from 0.4 to 0.8 as optimal for this dataset, and 0.6 was selected for further analysis. Assigning clusters identity was performed based on the canonical markers from literature-curated and statistically ranked genes. Differential expression analysis was performed using Model-based Analysis of Single-cell Transcriptomics (MAST)⁸¹, and pathway enrichment analysis was based on REACTOME pathway database (ReactomePA version 1.44.0). Significantly enriched pathways were identified using a 5% false discovery rate cutoff, and the Benjamini–Hochberg method was used to adjust P values and their enrichment significance was quantified using $-\text{Log}_{10}$ of P value adjusted.

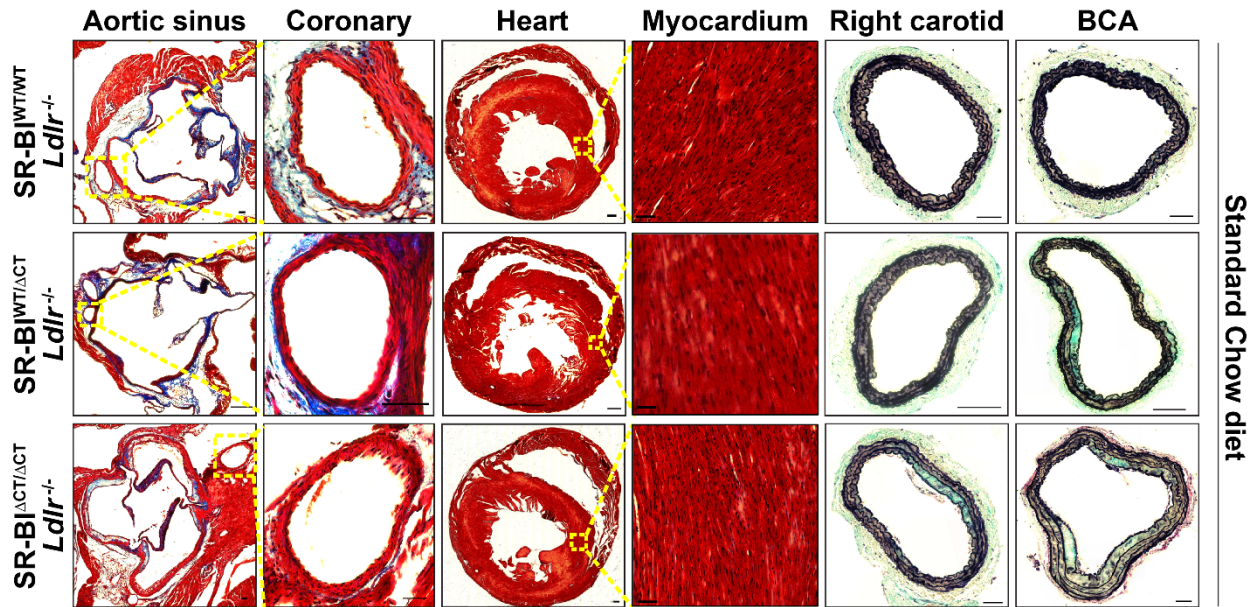


Figure S1: SR-BI^{ΔCT/ΔCT}/Ldlr^{-/-} mice fed a standard chow diet show no coronary atherosclerosis or spontaneous myocardial infarction. The hearts and associated vasculature, including coronary arteries, carotid arteries, and brachiocephalic arteries (BCAs), were collected from SR-BI^{WT/WT}/Ldlr^{-/-} (**top** row; n=9), SR-BI^{WT/ΔCT}/Ldlr^{-/-} (**middle** row; n=10) and SR-BI^{ΔCT/ΔCT}/Ldlr^{-/-} (**bottom** row; n=10) after 26 weeks feeding of a standard chow diet. Sections (10 μm) from the tissues were cut and stained with Masson's trichrome (aortic sinus, coronary artery, whole heart, myocardium) or Movat pentachrome (right carotid, BCA). Representative images are shown (panels **1** through **6** from **left** to **right**). The **first** column of panels show aortic sinuses (scale bars=200 μm) and magnified view of coronary arteries from the regions in the yellow boxes are shown in the **second** column of panels (scale bars=50 μm). Heart cross sections (left and right ventricular chambers appear white) are shown in the **third** column of panels (scale bars=500 μm) and higher magnification views of sections of myocardium (yellow boxes) are shown in the **fourth** column of panels (scale bars=50 μm). Right carotid arteries and BCAs are shown in the **fifth** and **sixth** columns of panels, respectively (scale bars=100 μm).

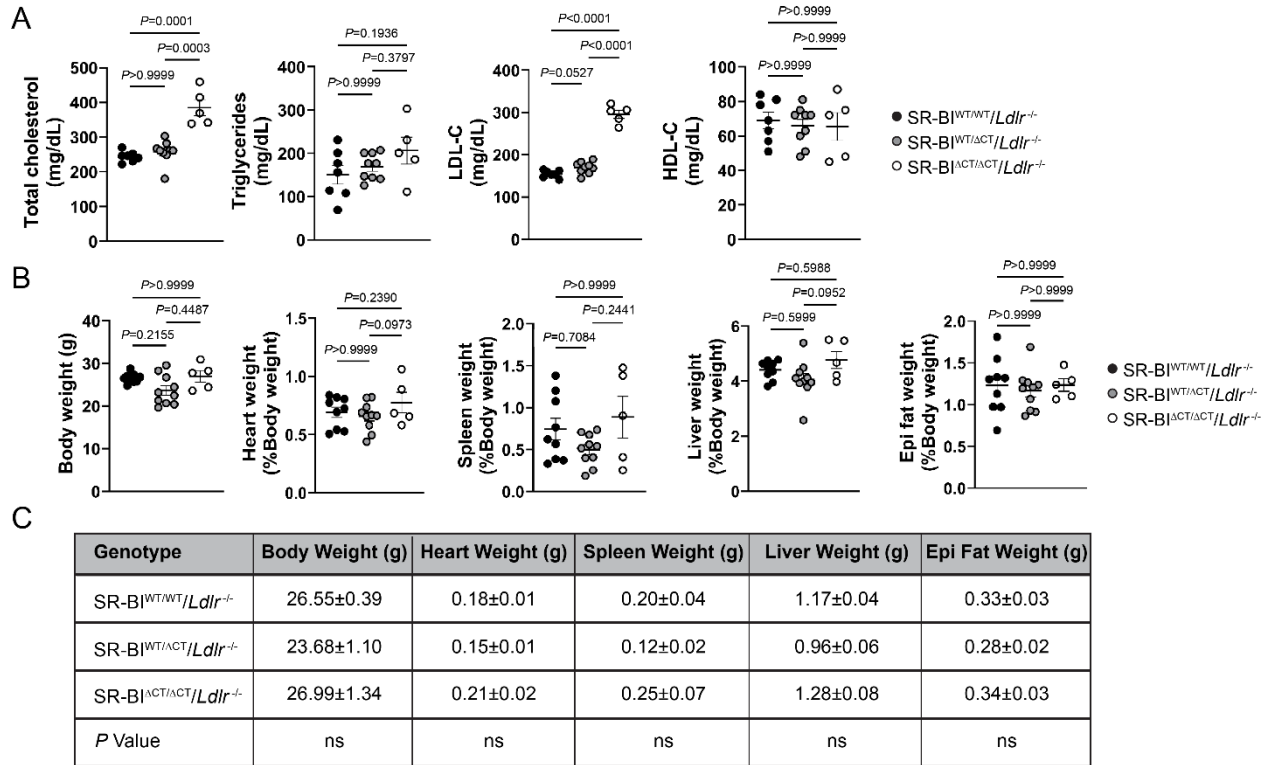


Figure S2: Analysis of plasma lipids and organ weights of SR-BI^{WT/WT}/Ldlr^{-/-}, SR-BI^{WT/ΔCT}/Ldlr^{-/-} and SR-BI^{ΔCT/ΔCT}/Ldlr^{-/-} mice fed a standard chow diet for 26 weeks. (A) Plasma levels of total cholesterol, triglycerides, apparent low-density lipoprotein cholesterol (LDL-C), and apparent high-density lipoprotein cholesterol (HDL-C) in SR-BI^{WT/WT}/Ldlr^{-/-} (black solid circles; n=7), SR-BI^{WT/ΔCT}/Ldlr^{-/-} (grey solid circles; n=9) and SR-BI^{ΔCT/ΔCT}/Ldlr^{-/-} (open circles; n=5) mice fed a standard chow diet for 26 weeks (see Results for description of apparent cholesterol concentrations). **(B and C)** Body and heart, spleen, liver and epididymal (epi) fat weights (% of body weight in **B** and absolute weights in **C**) for SR-BI^{WT/WT}/Ldlr^{-/-} (black solid circles; n=9), SR-BI^{WT/ΔCT}/Ldlr^{-/-} (grey solid circles; n=10) and SR-BI^{ΔCT/ΔCT}/Ldlr^{-/-} (open circles; n=5) mice fed a standard chow diet for 26 weeks. Data are shown as mean±SEM. Statistical analyses were performed with two-way ANOVA followed by the Bonferroni method of multiple pairwise comparisons. ns Indicates not significant ($P>0.05$).

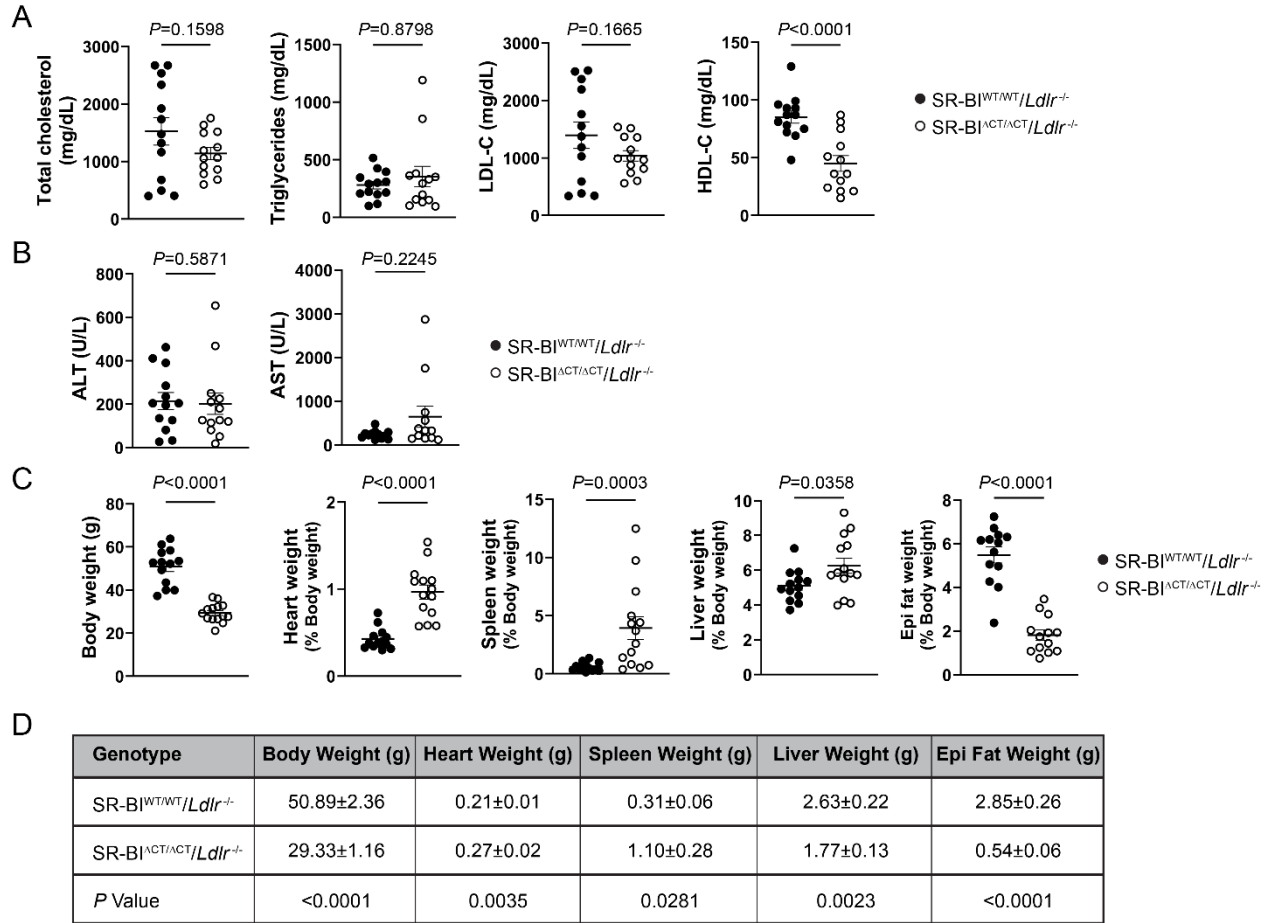


Figure S3: Analysis of plasma lipids, liver enzymes and organ weights of SR-BI^{WT/WT}/Ldlr^{-/-} and SR-BI^{ΔCT/ΔCT}/Ldlr^{-/-} mice fed a Western diet for 26 weeks. (A and B) Plasma levels of total cholesterol, triglycerides, apparent low-density lipoprotein cholesterol (LDL-C), apparent high-density lipoprotein cholesterol (HDL-C) (A) (see Results for description of apparent cholesterol concentrations), and the liver enzymes alanine transaminase (ALT) and aspartate transaminase (AST) (B) in SR-BI^{WT/WT}/Ldlr^{-/-} (solid black circles; n=13) and SR-BI^{ΔCT/ΔCT}/Ldlr^{-/-} (open circles; n=13) mice fed a Western diet (WD) for 26 weeks. (C and D) Body and heart, spleen, liver and epididymal (epi) fat weights (% of body weight in C and absolute weights in D) for SR-BI^{WT/WT}/Ldlr^{-/-} (solid black circles; n=13) and SR-BI^{ΔCT/ΔCT}/Ldlr^{-/-} (open circles; n=14) mice fed the WD for 26 weeks. Data are shown as mean±SEM. Statistical analyses were performed with unpaired Student *t* test (with Welch correction when variance was unequal) and unpaired Mann-Whitney *U* test.

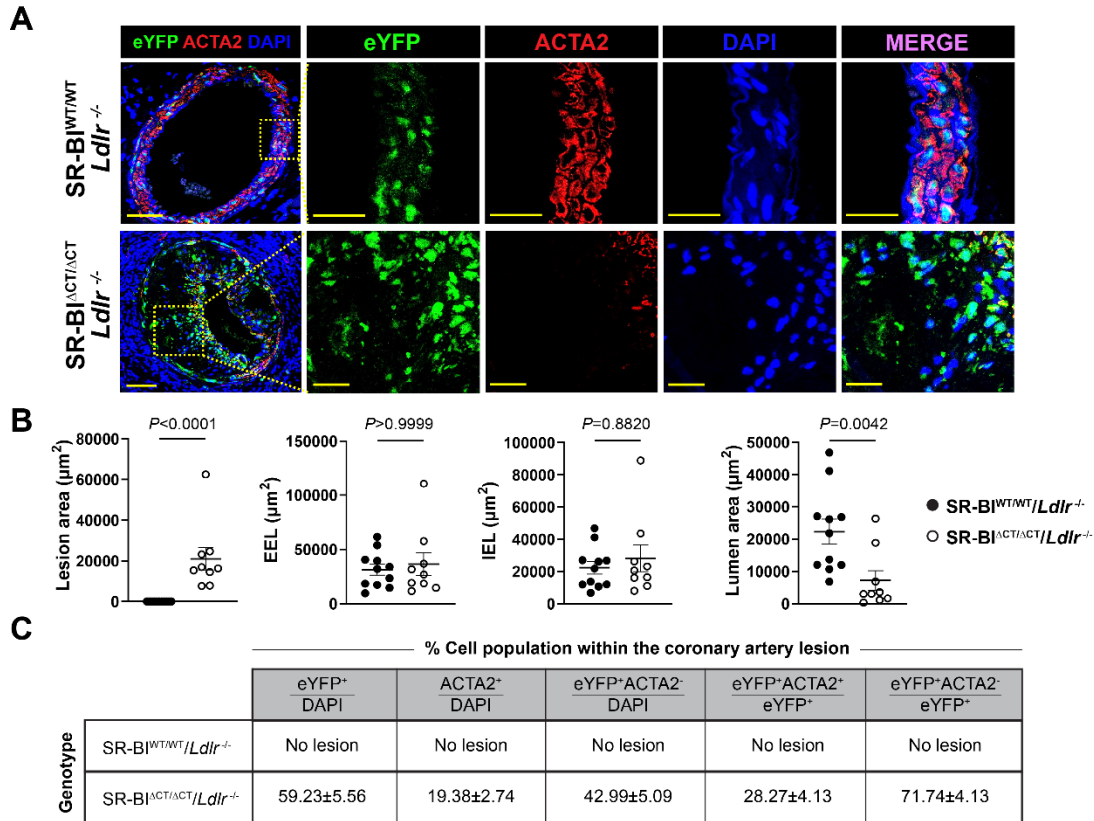


Figure S4: Analysis of smooth muscle cell lineage tracing in coronary artery atherosclerotic lesions in SR-BI^{WT/WT}/Ldlr^{-/-} and SR-BI^{ΔCT/ΔCT}/Ldlr^{-/-} mice fed a Western diet for 26 weeks.

(A, panels 1 through 5 from left to right) Representative immunofluorescent images of coronary arteries stained for eYFP (enhanced yellow fluorescent protein, SMC lineage tracing marker; panel 2), ACTA2 (smooth muscle alpha actin; panel 3), and fluorescence of DAPI (nuclei; panel 4) and merged fluorescence images (panels 1 and 5) at low (panel 1; scale bars=50 μ m) and high magnification (panels 2 through 5; scale bars=20 μ m). (B) Quantification of coronary artery lesion area, external elastic lamina area (EEL), internal elastic lamina area (IEL) and lumen area from 26-week Western diet (WD)-fed SR-BI^{WT/WT}/Ldlr^{-/-} (solid black circles; n=11) or SR-BI^{ΔCT/ΔCT}/Ldlr^{-/-} mice (open circles; n=9). (C) Analysis of the percent of total lesion cells derived from SMCs (eYFP⁺/DAPI), percent of total ACTA2⁺ lesion cells (ACTA2⁺/DAPI), percent of total lesion cells that are phenotypically modulated SMCs (eYFP⁺ACTA2⁺/DAPI), percent of total smooth muscle derived cells that are ACTA2⁺ (eYFP⁺ACTA2⁺/eYFP⁺) and the percent of total smooth muscle derived cells that are ACTA2⁻ (eYFP⁺ACTA2⁻/eYFP⁺) in coronary lesions from 26-week WD-fed SR-BI^{WT/WT}/Ldlr^{-/-} (n=8) or SR-BI^{ΔCT/ΔCT}/Ldlr^{-/-} mice (n=8). Data are shown as mean±SEM. Statistical analyses were performed with unpaired Mann-Whitney *U* test.

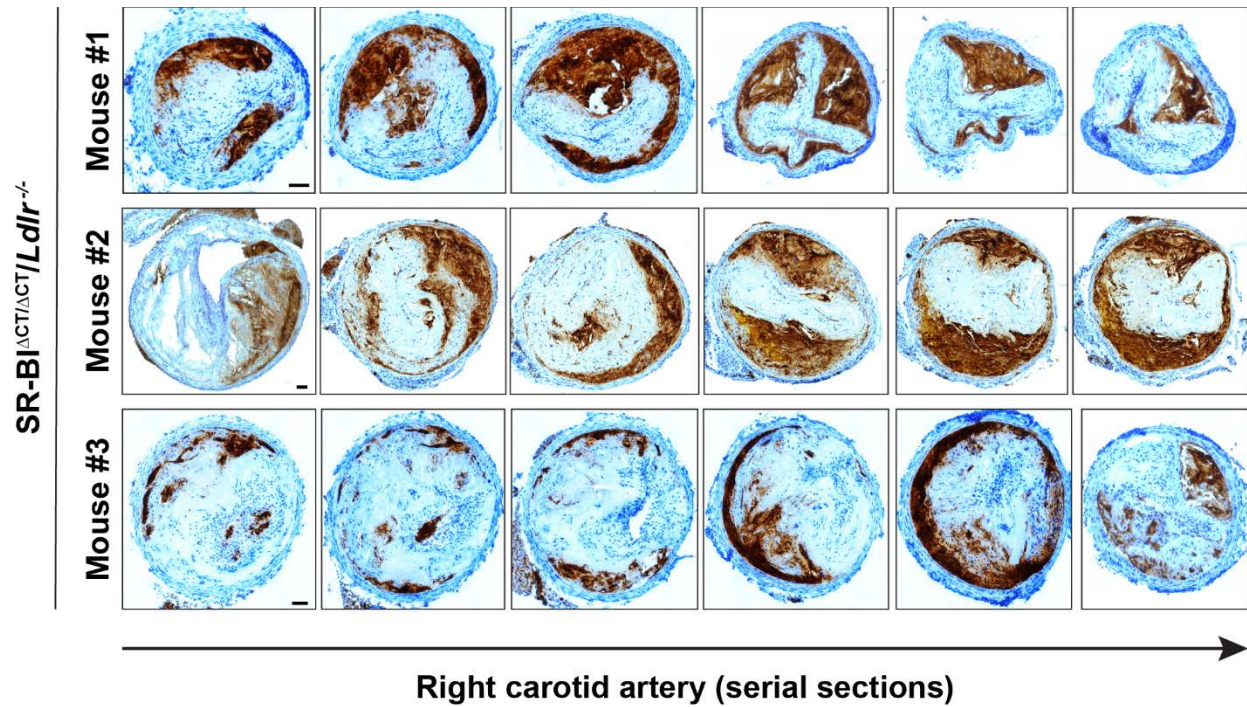


Figure S5: Analysis of plaque rupture in serial sections from right carotid artery atherosclerotic lesions in Western diet-fed SR-BI Δ CT/ Δ CT/*Ldlr* $^{-/-}$ mice. Ter-119 staining that detects plaque rupture/intraplaque hemorrhage (brown staining) of six serial sections from each of three independent SR-BI Δ CT/ Δ CT/*Ldlr* $^{-/-}$ mice fed Western diet (WD) for 26 weeks. All mice show complex, near complete or completely occluded right carotid vessels with multiple thrombi as shown by Ter-119 positive staining (brown staining; scale bars=50 μ m).

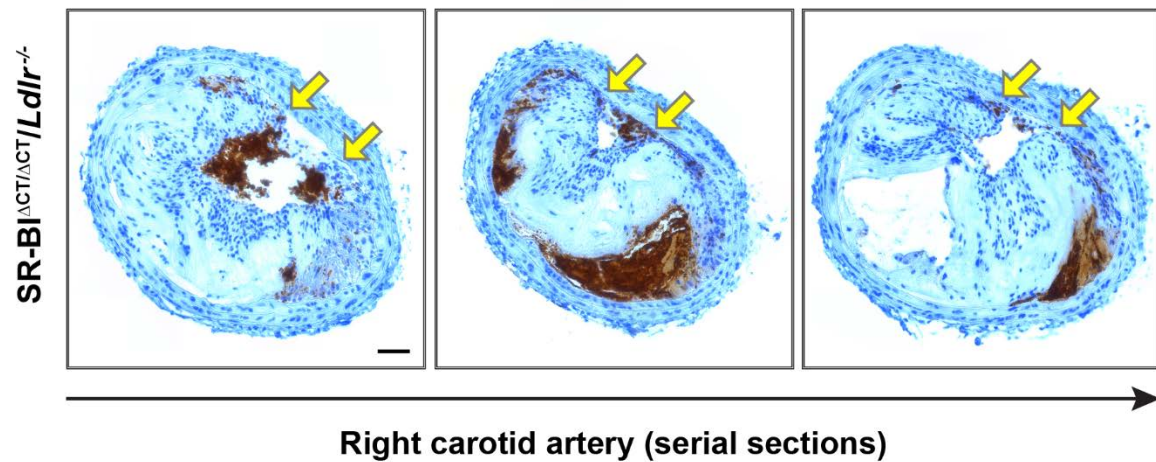


Figure S6: Organized luminal thrombi at the shoulder region of an atherosclerotic lesion with fibrous cap disruption in serial sections from a Western diet-fed SR-BI^{ΔCT/ΔCT}/Ldlr^{-/-} mouse. Ter-119 staining that detects plaque rupture/intraplaque hemorrhage (brown staining) of three serial sections from an SR-BI^{ΔCT/ΔCT}/Ldlr^{-/-} mouse fed Western diet (WD) for 26 weeks. The yellow arrows point to areas where thrombi have formed at the shoulder region of the plaque where there appears to be disruption of the fibrous cap (**left** panel; scale bar=50 μm).

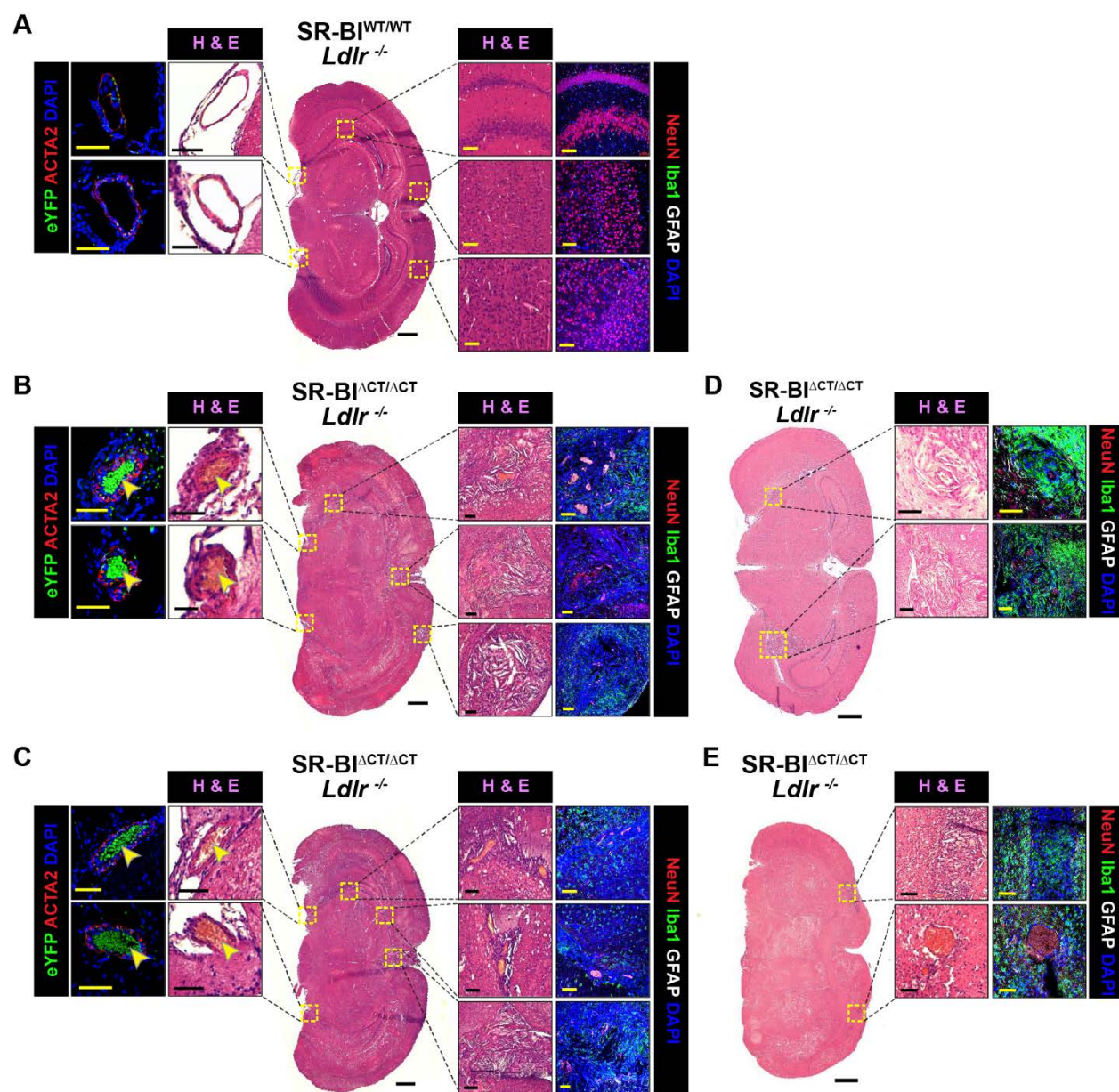


Figure S7

Figure S7: Histological analysis of brain sections from SR-BI^{WT/WT}/*Ldlr*^{-/-} and SR-BI ^{Δ CT/ Δ CT}/*Ldlr*^{-/-} mice fed a Western diet for 26 weeks. Representative coronal sections of brains from (A) SR-BI^{WT/WT}/*Ldlr*^{-/-} (n=15) and (B through E) SR-BI ^{Δ CT/ Δ CT}/*Ldlr*^{-/-} mice (n=16) fed a WD for 26 weeks. **Center** panels show low magnification images of brain sections stained with H&E (scale bars=500 μ m). Yellow squares highlight areas of tissue damage shown at high magnification in the indicated adjacent images (scale bars=50 μ m). Adjacent panels to the **right** show H&E staining as well as immunofluorescence staining using antibodies to the pan neuronal nuclear marker NeuN (neuronal nuclei), the microglial marker Iba1 (ionized calcium-binding adaptor molecule-1) and the astrocyte marker GFAP (glial fibrillary acidic protein), and fluorescence staining with DAPI (nuclei) (scale bars=50 μ m). Adjacent panels to the **left** (A through C) show cerebral vessels stained with H&E or immunofluorescence staining using antibodies to ACTA2 (smooth muscle alpha actin) and eYFP (enhanced yellow fluorescent protein, smooth muscle lineage tracing marker), and fluorescence of DAPI (nuclei) (scale bars=50 μ m). Yellow arrowheads point to autofluorescence from erythrocytes accumulated inside cerebral vessels (B and C).

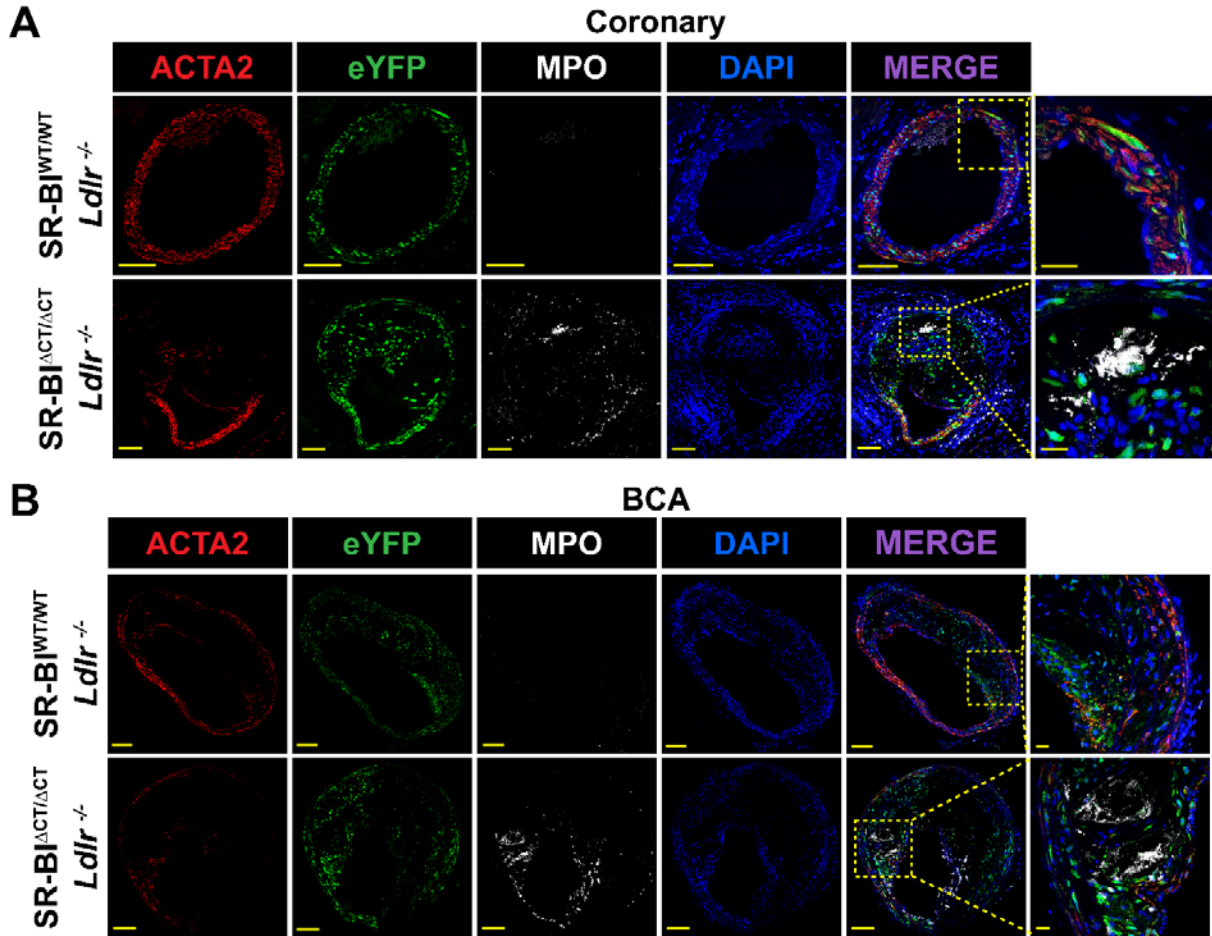


Figure S8: Immunofluorescence analysis of MPO expression in coronary and brachiocephalic arteries of SR-BI^{WT/WT}/*Ldlr*^{-/-} and SR-BI^{ΔCT/ΔCT}/*Ldlr*^{-/-} mice fed a Western diet for 26 weeks. (A through B, panels 1 through 6 from left to right) Representative immunofluorescence images of ACTA2 (smooth muscle alpha actin; panel 1), eYFP (enhanced yellow fluorescent protein, smooth muscle lineage tracing marker; panel 2), and MPO (myeloperoxidase; panel 3), and fluorescence of DAPI (nuclei; panel 4) and merged fluorescence images (panel 5 and 6) at low (panels 1 through 5) and high magnification (panel 6) in (A) coronary arteries (scale bars=50 μm for panels 1 through 5; scale bars=20 μm for panel 6) and (B) brachiocephalic arteries (BCAs; scale bars=100 μm for panels 1 through 5; scale bars=20 μm for panel 6) from WD-fed SR-BI^{WT/WT}/*Ldlr*^{-/-} (top panels; n=12) and SR-BI^{ΔCT/ΔCT}/*Ldlr*^{-/-} mice (bottom panels; n=14).

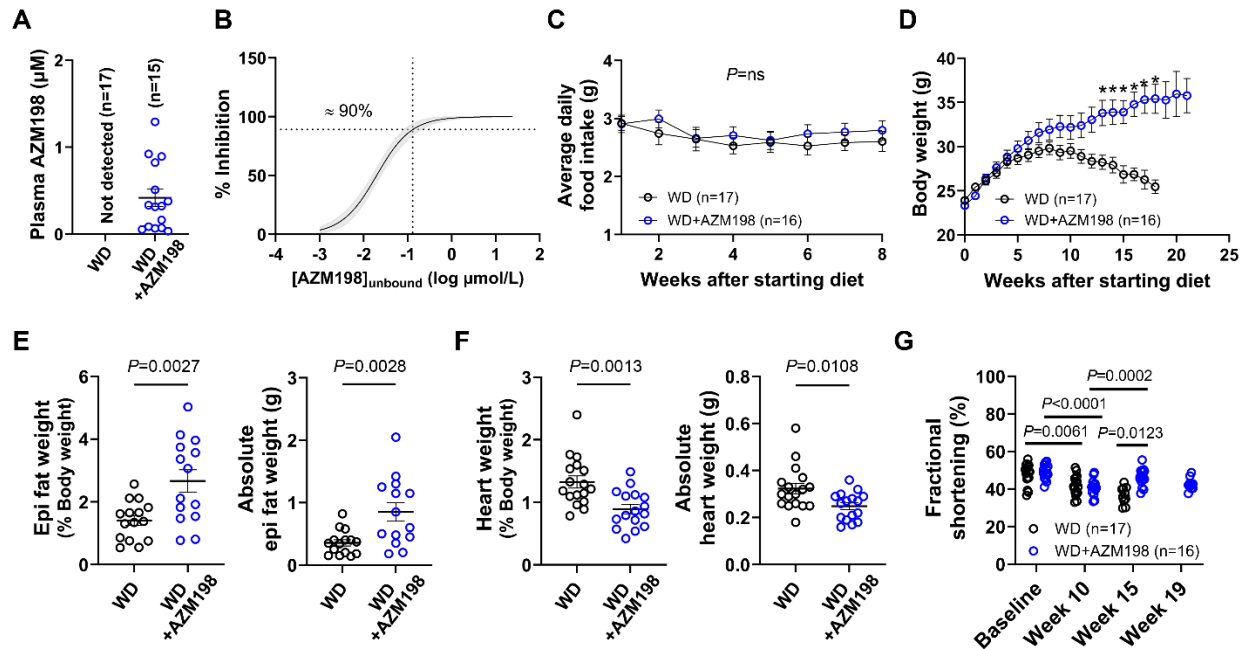


Figure S9: AZM198 improved heart function in SR-BI^{ΔCT/ΔCT}/Ldlr^{-/-} mice fed a Western diet. SR-BI^{ΔCT/ΔCT}/Ldlr^{-/-} mice were fed a Western diet (WD) (black circles) or WD+AZM198 (blue circles) for the indicated times. **(A)** Plasma AZM198 levels (WD, n=17; WD+AZM198, n=15). **(B)** Predicted MPO inhibition based on the previously reported potency of AZM198 on purified human MPO *in vitro*.⁵⁵ The solid line and shaded area represent the modelled and 95% confidence interval of the concentration-inhibition curve. The dashed lines represent the predicted inhibition associated with the unbound fraction of the mean plasma concentration of AZM198 (shown in A) from WD+AZM198-fed mice. **(C)** Average daily food intake (WD, n=17; WD+AZM198, n=16). **(D)** Body weights (WD, n=17; WD+AZM198, n=16). * $P<0.05$. **(E)** Epididymal (Epi) fat weights (% of body weight [left] and absolute weights [right]) (WD, n=15; WD+AZM198, n=14). **(F)** Heart weights (% of body weight [left] and absolute weights [right]) (WD, n=17; WD+AZM198, n=16). **(G)** Fractional shortening of hearts from sequential echocardiographic analysis (WD, n=17; WD+AZM198, n=16). Error bars represent mean \pm SEM. Statistical analyses were performed with unpaired Student *t* test (**A**, **E** through **F**) and mixed-effects ANOVA followed by the Sidak method of multiple pairwise comparisons (**C**, **D** and **G**).



Figure S10

Figure S10: AZM198 substantially shifts hepatic lipid composition in SR-BI^{ΔCT/ΔCT}/*Ldlr*^{-/-} mice, increasing phosphatidylethanolamines and sphingomyelins synthesis at the expense of phosphatidylcholines and ceramides. SR-BI^{ΔCT/ΔCT}/*Ldlr*^{-/-} mice were fed either WD (n=5) or WD+AZM198 (n=5) for 8 weeks and livers were collected, snap frozen and processed for lipidomic analysis. **(A)** Volcano plot illustrating the most highly increased and decreased lipid species in livers of mice fed WD+AZM198 compared to mice fed WD diets (X-axis: Log₂[Fold Change]; Y-axis: -Log₁₀[*P* value]). Red dots indicate the lipid species significantly enriched in the WD+AZM198-fed group while green dots indicate the lipid species significantly enriched in the WD-fed control group. **(B)** Top 20 most significantly changed hepatic lipids by fold change from the WD+AZM198-fed group compared to the WD-fed control group (enriched species in red, reduced in green). **(C)** Heatmap showing differentially abundant phospholipid species (by Z-score; enriched in WD+AZM198 vs WD), focused on statistically significantly changed phosphatidylcholine (PC) and phosphatidylethanolamine (PE) species. **(D)** Heatmap showing differentially abundant ceramide and sphingomyelin species (by Z-score; enriched in WD+AZM198 vs WD), focused on statistically significantly changed species. **(E)** Assignment of significantly changed lipids by KEGG pathway annotation. Number of significantly changed lipids is shown, followed in parentheses by the percent changed of all annotated lipids within a KEGG sub-pathway.

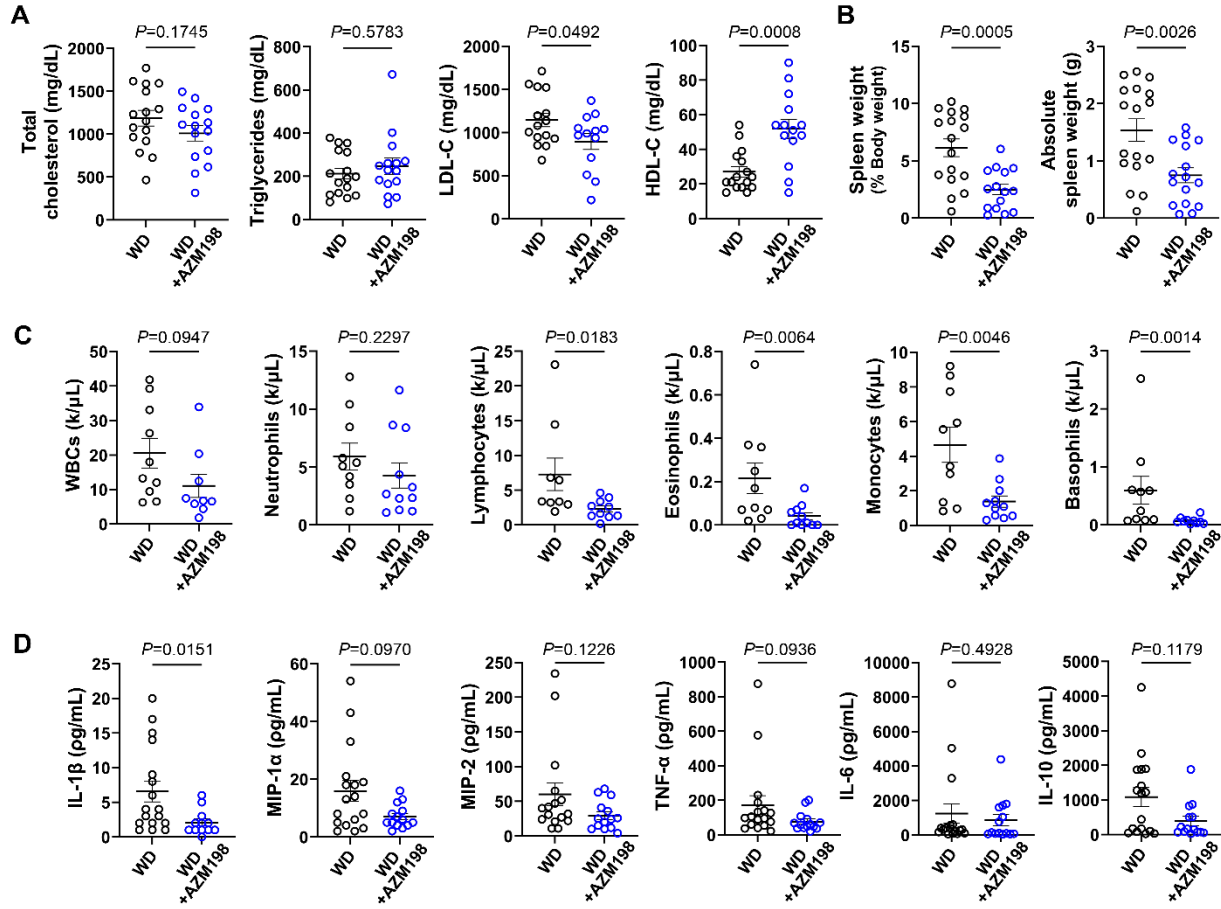


Figure S11: Effects of AZM198 on plasma lipids, cytokines, circulating immune cells, and spleens in SR-BI^{ΔCT/ΔCT}/Ldlr^{-/-} mice fed a Western diet. SR-BI^{ΔCT/ΔCT}/Ldlr^{-/-} mice were fed either a Western diet (WD) (black circles) or WD+AZM198 (blue circles) for 26 weeks. **(A)** Plasma total cholesterol, triglycerides, apparent low-density lipoprotein cholesterol (LDL-C), and apparent high-density lipoprotein cholesterol (HDL-C) (WD, n=16; WD+AZM198, n=16) (see Results for description of apparent cholesterol concentrations). **(B)** Spleen weights (% of body weight [left] and absolute weights [right]) (WD, n=17; WD+AZM198, n=16). **(C)** Concentrations of blood cells: white blood cells (WBCs), neutrophils, lymphocytes, monocytes, eosinophils, and basophils (WD, n=10; WD+AZM198, n=9). **(D)** Cytokine concentrations in plasma (WD, n=16; WD+AZM198, n=14). Error bars represent mean \pm SEM. Statistical analyses were performed with unpaired Mann-Whitney *U* test or Student *t* test (with Welch correction when variance was unequal). IL-1 β , interleukin-1 beta; IL-6, interleukin-6; IL-10, interleukin-10; MIP-1 α , macrophage inflammatory protein-1 alpha; MIP-2, macrophage inflammatory protein-2; TNF- α , tumor necrosis factor alpha.

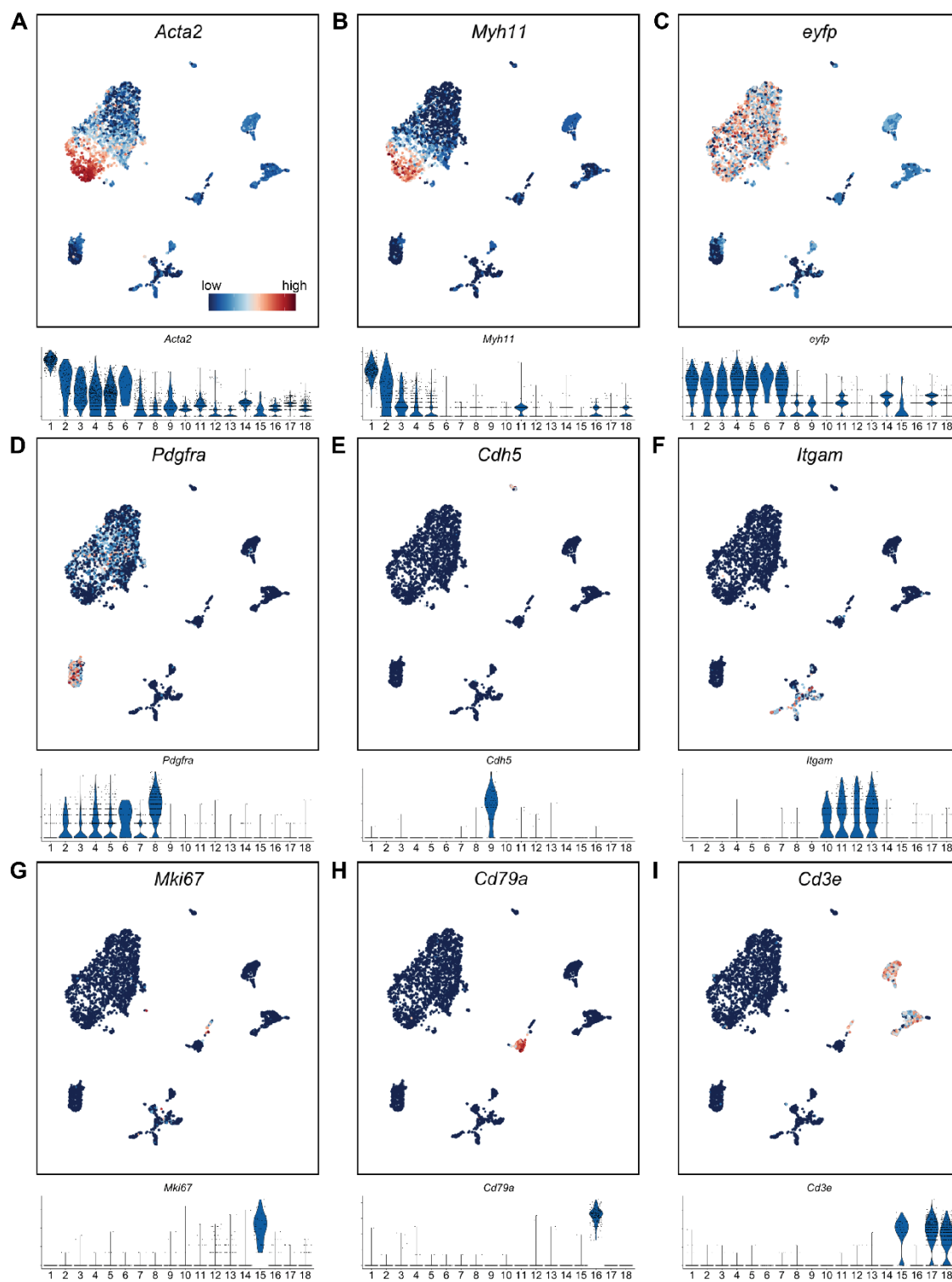


Figure S12

Figure S12: Classification of cell types in the atherosclerotic brachiocephalic artery (BCA) regions determined by single cell RNA sequencing (scRNA-seq) and expression of representative canonical marker genes. Samples of BCA regions from 3 mice for each condition (WD or WD+AZM198) were pooled into one group each and subsequently analyzed. After generation of single cells from the tissue, samples of either the entire population of single cells (unsorted cells) or eYFP (enhanced yellow fluorescent protein) positive cells (smooth muscle cells [SMCs], eYFP⁺ sorted cells) were subjected to scRNA-seq analysis and results were analyzed using UMAP plots (**top**) and violin plots for the 18 cell clusters (**bottom**) for individual cell-type marker genes as described in Figure 8. The genes analyzed were: *Acta2* (**A**) and *Myh11* (**B**) which are SMC marker genes, *Eyfp* (**C**) which identifies all cells derived from SMC lineage, *Pdgfra* (**D**) which is a fibroblast marker gene, *Cdh5* (**E**) which is an endothelial cell marker gene, *Itgam* (**F**) (also known as *CD11b*) which is a macrophage marker gene, *Mki67* (**G**) which is a marker gene for proliferating cells, *CD79a* (**H**) which is a B-cell marker gene, and *Cd3e* (**I**) which is a T-cell marker gene.

Video S1: A representative WD-fed SR-BI^{ΔCT/ΔCT}/*Ldlr*^{-/-} mouse displaying head tilt and spinning which are symptoms of stroke.

Video S2: A representative WD-fed SR-BI^{ΔCT/ΔCT}/*Ldlr*^{-/-} mouse displaying hind limb paralysis which is a symptom of stroke.

Video S3: A representative WD-fed SR-BI^{WT/WT}/*Ldlr*^{-/-} mouse displaying no neurological symptoms of stroke.

Major Resources Table

In order to allow validation and replication of experiments, all essential research materials listed in the Methods should be included in the Major Resources Table below. Authors are encouraged to use public repositories for protocols, data, code, and other materials and provide persistent identifiers and/or links to repositories when available. Authors may add or delete rows as needed.

Animals (in vivo studies)

Species	Vendor or Source	Background Strain	Sex	Persistent ID / URL
<i>Myh11-CreER^{T2}/ROSA26 STOP^{FL/FL}-eYFP^{+/+}</i>	Owens Lab	C57BL/6	M: Cre+ F: Cre-	https://www.nature.com/articles/nmeth.2332
SR-BI ^{ΔCT} / <i>Ldlr</i> KO	The Jackson Laboratory	C57BL/6 & 129S	M & F	https://www.jax.org/strain/033709
<i>Myh11-CreER^{T2}-eYFP SR-BI^{WT/WT}/<i>Ldlr</i>^{-/-}</i>	Owens Lab	C57BL/6 & 129S	M: Cre+ F: Cre-	
<i>Myh11-CreER^{T2}-eYFP SR-BI^{WT/ΔCT}/<i>Ldlr</i>^{-/-}</i>	Owens Lab	C57BL/6 & 129S	M: Cre+ F: Cre-	
<i>Myh11-CreER^{T2}-eYFP SR-BI^{ΔCT/ΔCT}/<i>Ldlr</i>^{-/-}</i>	Owens Lab	C57BL/6 & 129S	M: Cre+ F: Cre-	

Genetically Modified Animals

		Species	Vendor or Source	Back ground Strain	Other Info	Persistent ID / URL
<i>Myh11-CreER^{T2}-eYFP SR-BI^{WT/ΔCT}/<i>Ldlr</i>^{-/-}</i>	Parent - Male	<i>Myh11-CreER^{T2}-eYFP</i>	Owens Lab	C57BL/6		https://www.nature.com/articles/nmeth.2332
	Parent - Female	SR-BI ^{ΔCT} / <i>Ldlr</i> KO	The Jackson Laboratory	C57BL/6 & 129S		https://www.jax.org/strain/033709
<i>Myh11-CreER^{T2}-eYFP SR-BI^{ΔCT/ΔCT}/<i>Ldlr</i>^{-/-} & <i>Myh11-CreER^{T2}-eYFP SR-BI^{WT/WT}/<i>Ldlr</i>^{-/-}</i></i>	Parent - Male	<i>Myh11-CreER^{T2}-eYFP SR-BI^{WT/ΔCT}/<i>Ldlr</i>^{-/-}</i>	Owens Lab	C57BL/6 & 129S		
	Parent - Female	<i>Myh11-CreER^{T2}-eYFP SR-BI^{WT/ΔCT}/<i>Ldlr</i>^{-/-}</i>	Owens Lab	C57BL/6 & 129S		

Antibodies

Target antigen	Vendor or Source	Catalog #	Working concentration	Lot # (preferred but not required)	Persistent ID / URL
GFP	Abcam	ab6673	1:100		https://www.abcam.com/products/primary-antibodies/gfp-antibody-ab6673.html
GFP	Abcam	ab252881	1:200		https://www.abcam.com/products/primary-antibodies/gfp-antibody-3h9-ab252881.html
MPO	Abcam	ab208670	1:200		https://www.abcam.com/products/primary-antibodies/myeloperoxidase-antibody-epr20257-ab208670.html
MPO	Abcam	ab16886	1:200		https://www.abcam.com/products/primary-antibodies/myeloperoxidase-antibody-8f4-ab16886.html
MPO	R&D	AF3667	1:200		https://www.rndsystems.com/products/human-mouse-myeloperoxidase-mpo-antibody_af3667?gad_source=1&gclid=Cj0KCQjwqpSwBhClARIsADlZ_TlGK79olpafVLrZoigjJQvaX7iC7V4OkeOSvAsab6Sd3hrRPYhgy1YaAvNnEALw_wcB&gclid=aw.ds#product-datasheets
Cit-H3	Abcam	ab281584	1:200		https://www.abcam.com/products/primary-antibodies/histone-h3-citrulline-r2-r8-r17-antibody-rm1001-ab281584.html
FITC-conjugated ACTA2 (clone 1A4)	Sigma	F3777	1:500		https://www.sigmaaldrich.com/US/en/product/sigma/f3777
NeuN	Abcam	ab177487	1:500		https://www.abcam.com/products/primary-antibodies/neun-antibody-epr12763-neuronal-marker-ab177487.html
Iba1	Fujifilm Wako	013-27691	1:500		https://labchem-wako.fujifilm.com/us/product/detail/W01W0101-2769.html
GFAP	Abcam	ab7260	1:500		https://www.abcam.com/products/primary-antibodies/gfap-antibody-ab7260.html

GFAP	Abcam	Ab4674	1:500		https://www.abcam.com/products/primary-antibodies/gfap-antibody-ab4674.html
Ter-119	Santa Cruz Biotechnology	sc-19592	1:200		https://www.scbt.com/p/erythroid-lineage-antibody-ter-119
Donkey anti-rabbit Alexa Fluor 488	Thermo Fisher Scientific	A21206	1:250		https://www.thermofisher.com/antibody/product/Donkey-anti-Rabbit-IgG-H-L-Highly-Cross-Adsorbed-Secondary-Antibody-Polyclonal/A-21206
Donkey anti-rabbit Alexa Fluor 546	Thermo Fisher Scientific	A10040	1:250		https://www.thermofisher.com/antibody/product/Donkey-anti-Rabbit-IgG-H-L-Highly-Cross-Adsorbed-Secondary-Antibody-Polyclonal/A10040
Donkey anti-goat Alexa Fluor 647	Thermo Fisher Scientific	A21447	1:250		https://www.thermofisher.com/antibody/product/Donkey-anti-Goat-IgG-H-L-Cross-Adsorbed-Secondary-Antibody-Polyclonal/A-21447
Donkey anti-chicken Alexa Fluor 647	Jackson Immuno Research	703-605-155	1:250		https://www.jacksonimmuno.com/catalog/products/703-605-155

DNA/cDNA Clones

Clone Name	Sequence	Source / Repository	Persistent ID / URL

Cultured Cells

Name	Vendor or Source	Sex (F, M, or unknown)	Persistent ID / URL

Data & Code Availability

Description	Source / Repository	Persistent ID / URL
The data and code that support the findings of this study will be made publicly available prior to publication		

Other (Data acquisition and Analysis Software)

Description	Source / Repository	Persistent ID / URL
ZEN 2.3 SP1 FP3	ZEISS	https://www.micro-shop.zeiss.com/en/us/softwarefinder/software-categories/zen-black/zen-black-system/
Leica Application Suite X 3.7.2.22383	Leica Microsystems	https://www.leica-microsystems.com/products/microscope-software/p/leica-las-x-ls/
BD FACSTM Software 1.2.0.142	BD Biosciences	
NovaSeq 6000 Sequencing System	Illumina	https://www.illumina.com/systems/sequencing-platforms/novaseq.html
NovaSeq X Plus sequencing system	Illumina	https://www.illumina.com/systems/sequencing-platforms/novaseq-x-plus.html
GraphPad Prism 10.0	GraphPad Software	https://www.graphpad.com/
ImageJ 1.54f	NIH	https://imagej.net/ij/notes.html
CellRanger 6.0	10x Genomics	https://support.10xgenomics.com/single-cell-gene-expression/software/pipelines/latest/release-notes
RStudio 4.1	Posit	https://posit.co/download/rstudio-desktop/
Seurat 4.3	Satija Lab	https://satijalab.org/seurat/
ReactomePA 1.44	Bioconductor	https://bioconductor.org/packages/release/bioc/html/ReactomePA.html
MAST 1.25	Bioconductor	https://www.bioconductor.org/packages/release/bioc/html/MAST.html
Vevo LAB 3.1.0	VisualSonics, Fujifilm	https://www.visualsonics.com/product/software/vevo-lab

ARRIVE GUIDELINES

The ARRIVE guidelines (<https://arriveguidelines.org/>) are a checklist of recommendations to improve the reporting of research involving animals. Key elements of the study design are included below to better enable readers to scrutinize the research adequately, evaluate its methodological rigor, and reproduce the methods or findings.

Study Design

Groups	Sex	Age (Week)	# Mice (prior to experiment)	# Mice (after termination)	Littermates (Yes/No)	Outcome Measures
<i>Myh11-CreER^{T2}-eYFP</i> SR-BI ^{WT/WT} / <i>Ldlr</i> ^{-/-} Group 1 (Chow Fed)	Male	35	9	9	Yes	Survival, histology, blood analyses
<i>Myh11-CreER^{T2}-eYFP</i> SR-BI ^{WT/ΔCT} / <i>Ldlr</i> ^{-/-} Group 2 (Chow Fed)	Male	35	10	10	Yes	Survival, histology, blood analyses
<i>Myh11-CreER^{T2}-eYFP</i> SR-BI ^{ΔCT/ΔCT} / <i>Ldlr</i> ^{-/-} Group 3 (Chow Fed)	Male	35	10	10	Yes	Survival, histology, blood analyses
<i>Myh11-CreER^{T2}-eYFP</i> SR-BI ^{WT/WT} / <i>Ldlr</i> ^{-/-} Group 1 (WD Fed)	Male	35	15	15	Yes	Survival, histology, blood analyses
<i>Myh11-CreER^{T2}-eYFP</i> SR-BI ^{WT/ΔCT} / <i>Ldlr</i> ^{-/-} Group 2 (WD Fed)	Male	35	7	7	Yes	Survival, histology, blood analyses
<i>Myh11-CreER^{T2}-eYFP</i> SR-BI ^{ΔCT/ΔCT} / <i>Ldlr</i> ^{-/-} Group 3 (WD Fed)	Male	35	16	16	Yes	Survival, histology, blood analyses

<i>Myh11-CreER^{T2}-eYFP</i> SR-BI ^{ΔCT/ΔCT} / <i>Ldlr</i> ^{-/-} Group 1 (Control WD Fed)	Male	35	17	17	Yes	Survival, histology, blood analyses, echocardiography, bulk RNAseq, lipidomics, scRNAseq
<i>Myh11-CreER^{T2}-eYFP</i> SR-BI ^{ΔCT/ΔCT} / <i>Ldlr</i> ^{-/-} Group 2 (WD+AZM198 Fed)	Male	35	16	16	Yes	Survival, histology, blood analyses, echocardiography, bulk RNAseq, lipidomics, scRNAseq

Sample Size

Sample size was determined by a priori power analysis using G*Power (<https://www.psychologie.hhu.de/arbeitsgruppen/allgemeine-psychologie-und-arbeitspsychologie/gpower.html>) based on the expected biological difference of 30% between experimental groups (accepting P% = 80 and α% = 5) and considering expected number of animals that could reach humane terminal end point prior to completion of 26 weeks of Western diet feeding.

Inclusion Criteria

Viable, healthy mice born at the University of Virginia MR5 animal vivarium and able to be genotyped by tail biopsy.

Exclusion Criteria

Exclusion criteria were pre-established to exclude animals that suffer from common mouse congenital/genetic abnormality (i.e. hydrocephalus, malocclusion) or do not show hyperlipidemia after Western diet (WD) feeding. For our study no animals required exclusion.

Randomization

Mice are assigned a 6-digit identification number prior to first genotyping. "*Myh11-CreER^{T2}-eYFP* SR-BI^{WT/WT}/*Ldlr*^{-/-}", "*Myh11-CreER^{T2}-eYFP* SR-BI^{WT/ΔCT}/*Ldlr*^{-/-}" and "*Myh11-CreER^{T2}-eYFP* SR-BI^{ΔCT/ΔCT}/*Ldlr*^{-/-}" littermate controls were used for all experiments. For experiments involving AZM198, "*Myh11-CreER^{T2}-eYFP* SR-BI^{ΔCT/ΔCT}/*Ldlr*^{-/-}" mice were randomly assigned to control (WD) or drug treated (WD+AZM198) group.

Blinding

Researchers were blinded to genotype or condition during data collection and analysis.

References

23. Alencar GF, Owsiany KM, Karnewar S, Sukhavasi K, Mocci G, Nguyen AT, Williams CM, Shamsuzzaman S, Mokry M, Henderson CA, et al. Stem Cell Pluripotency Genes Klf4 and Oct4 Regulate Complex SMC Phenotypic Changes Critical in Late-Stage Atherosclerotic Lesion Pathogenesis. *Circulation*. 2020;142:2045–2059.
24. Newman AA, Serbulea V, Baylis RA, Shankman LS, Bradley X, Alencar GF, Owsiany K, Deaton RA, Karnewar S, Shamsuzzaman S, et al. Multiple cell types contribute to the atherosclerotic lesion fibrous cap by PDGFR β and bioenergetic mechanisms. *Nat. Metab*. 2021;3:166–181.
29. Shankman LS, Gomez D, Cherepanova OA, Salmon M, Alencar GF, Haskins RM, Swiatlowska P, Newman AAC, Greene ES, Straub AC, et al. KLF4-dependent phenotypic modulation of smooth muscle cells has a key role in atherosclerotic plaque pathogenesis. *Nat. Med*. 2015;21:628–637.
44. Gomez D, Baylis RA, Durgin BG, Newman AAC, Alencar GF, Mahan S, St. Hilaire C, Müller W, Waisman A, Francis SE, et al. Interleukin-1 β has atheroprotective effects in advanced atherosclerotic lesions of mice. *Nat. Med*. 2018;24:1418–1429. 74. Cherepanova OA, Gomez D, Shankman LS, Swiatlowska P, Williams J, Sarmiento OF, Alencar GF, Hess DL, Bevard MH, Greene ES, et al. Activation of the pluripotency factor OCT4 in smooth muscle cells is atheroprotective. *Nat. Med*. 2016;22:657–665.
57. Rashid I, Maghazal GJ, Chen Y-C, Cheng D, Talib J, Newington D, Ren M, Vajandar SK, Searle A, Maluenda A, et al. Myeloperoxidase is a potential molecular imaging and therapeutic target for the identification and stabilization of high-risk atherosclerotic plaque. *Eur. Heart J*. 2018;39:3301–3310.

77. Percie du Sert N, Hurst V, Ahluwalia A, Alam S, Avey MT, Baker M, Browne WJ, Clark A, Cuthill IC, Dirnagl U, et al. The ARRIVE guidelines 2.0: Updated guidelines for reporting animal research. *Br J Pharmacol*. 2020 Aug;177(16):3617-3624.
78. Cherepanova OA, Gomez D, Shankman LS, Swiatlowska P, Williams J, Sarmento OF, Alencar GF, Hess DL, Bevard MH, Greene ES, et al. Activation of the pluripotency factor OCT4 in smooth muscle cells is atheroprotective. *Nat. Med*. 2016;22:657–665.
79. Hafemeister C, Satija R. Normalization and variance stabilization of single-cell RNA-seq data using regularized negative binomial regression. *Genome Biol*. 2019;20:296.
80. Patterson-Cross RB, Levine AJ, Menon V. Selecting single cell clustering parameter values using subsampling-based robustness metrics. *BMC Bioinformatics*. 2021;22:39.
81. Finak G, McDavid A, Yajima M, Deng J, Gersuk V, Shalek AK, Slichter CK, Miller HW, McElrath MJ, Prlic M, et al. MAST: a flexible statistical framework for assessing transcriptional changes and characterizing heterogeneity in single-cell RNA sequencing data. *Genome Biol*. 2015;16:278.